International Journal of Applied Earth Observations and Geoinformation 112 (2022) 102866

Contents lists available at ScienceDirect

International Journal of Applied Earth Observations and Geoinformation

journal homepage: www.elsevier.com/locate/jag

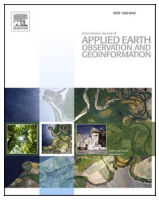

Monitoring peatland water table depth with optical and radar satellite imagery

Aleksi Räsänen [a,*], Anne Tolvanen [a], Santtu Kareksela [b,c]

[a] Natural Resources Institute Finland (Luke), Paavo Havaksen tie 3, FI-90570 Oulu, Finland
[b] Metsähallitus, Parks & Wildlife Finland, Vankanlähde 7, FI-13100 Hämeenlinna, Finland
[c] JYU.Wisdom, P.O. Box 35, FI-40014 University of Jyväskylä, Jyväskylä, Finland

ARTICLE INFO

Keywords:
Optical satellite imagery
Peatland
Soil moisture
Synthetic aperture radar
Wetland
Wetness

ABSTRACT

Peatland water table depth (WTD) and wetness have widely been monitored with optical and synthetic aperture radar (SAR) remote sensing but there is a lack of studies that have used multi-sensor data, i.e., combination of optical and SAR data. We assessed how well WTD can be monitored with remote sensing data, whether multi-sensor approach boosts explanatory capacity and whether there are differences in regression performance between data and peatland types. Our data consisted of continuous multiannual WTD data from altogether 50 restored and undrained Finnish peatlands, and optical (Landsat 5–8, Sentinel-2) and Sentinel-1 C-band SAR data processed in Google Earth Engine. We calculated random forest regressions with dependent variable being WTD and independent variables consisting of 21 optical and 10 SAR metrics. The average regression performance was moderate in multi-sensor models (R^2 43.1%, nRMSE 19.8%), almost as high in optical models (R^2 42.4%, nRMSE 19.9%) but considerably lower in C-band SAR models (R^2 21.8%, nRMSE 23.4%) trained separately for each site. When the models included data from several sites but were trained separately for six habitat type and management option combinations, the average R^2 was 40.6% for the multi-sensor models, 36.6% for optical models and 33.7% for C-band SAR models. There was considerable site-specific variation in the model performance (R^2 −3.3–88.8% in the multi-sensor models ran separately for each site) and whether multi-sensor, optical or C-band SAR model performed best. The average regression performance was higher for undrained than for restored peatlands, and higher for open and sparsely treed than for densely treed peatlands. The most important variables included SWIR-based optical metrics and VV SAR backscatter. Our results suggest that optical data works usually better than does C-band SAR data in peatland WTD monitoring and multi-sensor approach increases explanatory capacity moderately little.

1. Introduction

Boreal peatlands are under change because of human-induced drying, degradation and restoration, and there is a need to develop methods to monitor the state of peatlands and assess restoration success (Andersen et al., 2017; Chimner et al., 2017). As remote sensing provides objective spatially explicit and temporally extensive data, it has been suggested to be a useful method for peatland monitoring (Chasmer et al., 2020a, 2020b).

A key parameter for peatland ecosystem functioning is water table depth (WTD), i.e., how close to the surface the water body in the peat pool reaches. In peatlands, WTD correlates with soil and surface moisture, especially just above the water table (Kellner and Halldin, 2002; Strack and Price, 2009; Lafleur et al., 2005).

So far, WTD, wetness and soil moisture have been monitored with different remote sensing sensors, including optical, thermal, passive microwave and active microwave (Babaeian et al., 2019; Li et al., 2021; Peng et al., 2021; Santi et al., 2016). The highest spatial resolution can be achieved with optical and active microwave such as synthetic aperture radar data (SAR), while passive microwave observations have low spatial resolution (Babaeian et al., 2019; Li et al., 2021; Peng et al., 2021) that hampers monitoring in peatlands due to their small size and spatial heterogeneity (Burdun et al., 2020; Kalacska et al., 2018; Burdun et al., 2020). Some studies have also indicated that optical indices outperform thermal ones in peatland wetness studies (Burdun et al., 2020). Indeed, development and research utilizing in particular SAR

* Corresponding author.
E-mail address: aleksi.rasanen@luke.fi (A. Räsänen).

https://doi.org/10.1016/j.jag.2022.102866
Received 21 February 2022; Received in revised form 8 June 2022; Accepted 9 June 2022
Available online 17 June 2022

data but also optical sensors has been widespread in soil moisture studies, also in peatlands. Furthermore, decadal satellite observations (e.g., NASA/USGS Landsat and MODIS) provide opportunities for monitoring the state of peatlands for long time periods while newer satellites such as Sentinel satellites provide high spatial and temporal resolution for the most recent past (El Hajj et al., 2017; Gao et al., 2017; Paloscia et al., 2013; Ambrosone et al., 2020; Sadeghi et al., 2017; Bauer-Marschallinger et al., 2018).

Of the optical bands and indices, shortwave infrared (SWIR) bands and indices have been shown to be promising in soil moisture detection. As SWIR reflectance is sensitive also to vegetation, SWIR-based wetness indices typically include also near-infrared (NIR) (Sadeghi et al., 2017; Wang and Qu, 2007; Gao, 1996), or visible light reflectance (Zhang et al., 2013). One of the most recent development has been the use of optical trapezoid model (OPTRAM) that utilizes normalized difference vegetation index (NDVI) as a measure of vegetation content and SWIR transformed reflectance (STR) as a measure of soil moisture. A two-dimensional STR-NDVI space, in which each pixel represents one observation, models soil moisture along varying vegetation content (Sadeghi et al., 2017). Studies in peatlands have shown that OPTRAM works well in WTD monitoring (Burdun et al., 2020; Burdun et al., 2020), but there are also other optical metrics that have been tested in peatland WTD or wetness detection. For instance, some studies have reported a high correlation between narrowband airborne or field spectroscopy-based SWIR-NIR indices and soil moisture or WTD (Kalacska et al., 2018; Meingast et al., 2014; Harris and Bryant, 2009). Some have also shown that MODIS NDVI is highly positively correlated with WTD (Šimanauskienė et al., 2019), whereas others have reported a negative correlation between MODIS NDVI and WTD (D'Acunha et al., 2018). The link between NDVI and WTD is probably indirect as NDVI is sensitive to changes in vegetation greenness, composition, and structure (McPartland et al., 2019). It has also been discussed that wet area development within peatland can be monitored with spaceborne visible and infrared bands (Kolari et al., 2021), while others have suggested that there are differences between study areas in which indices work best in wet area detection (Ludwig et al., 2019).

In SAR data analyses in peatlands, the use of Sentinel-1 C-band SAR data has increased during the last decade (Holtgrave et al., 2018; Dabrowska-Zielinska et al., 2018; Lees et al., 2021; Manninen et al., 2022; Asmuß et al., 2019) while also sensors such as C-band ENVISAT ASAR, C-band Radarsat, C-band ERS and L-band PALSAR have been used (Torbick et al., 2012; Bechtold et al., 2018; Millard et al., 2018; Millard and Richardson, 2018; Kim et al., 2017; Kasischke et al., 2009). It has been shown that various SAR polarizations, including those of Sentinel-1, i.e., vertical transmission combined with vertical reception (VV) or with horizontal reception (VH), and combinations of them are useful in wetness studies (Dabrowska-Zielinska et al., 2018; Lees et al., 2021; Asmuß et al., 2019). Some studies have assessed whether data from ascending or descending orbit functions better in WTD monitoring; in some studies, there have been small differences between the orbits (Asmuß et al., 2019; Bechtold et al., 2018) but other studies have found that ascending orbit functions better (Dabrowska-Zielinska et al., 2018). In addition to water and surface moisture, SAR backscatter is sensitive to surface and vegetation structure. Therefore, some of the SAR studies have used optical NDVI data to correct for vegetation effects in the SAR backscatter (Holtgrave et al., 2018; Dabrowska-Zielinska et al., 2018). Other studies have shown that vegetation effects can be compensated also with SAR-based calculations (Dabrowska-Zielinska et al., 2018; Manninen et al., 2022); in open peatlands, simple sine equations that model vegetation growth and senescence can also compensate for vegetation effects (Lees et al., 2021).

There is a lack of studies that test satellite imagery-based monitoring at different peatland habitat types under different management regimes. This is crucial, since peatland habitat types, ranging from densely treed to open peatlands, also differ in their trophic and moisture status (Chasmer et al., 2020a, 2020b). Furthermore, many of the peatlands have been heavily degraded due to drainage, and some of the degraded peatlands have been restored during the past decades (Andersen et al., 2017; Chimner et al., 2017), while other peatlands have not been actively drained (Kolari et al., 2021; Sallinen et al., 2019). The few multi-site studies have included < 20 study sites (Burdun et al., 2020; Holtgrave et al., 2018; Lees et al., 2021; Asmuß et al., 2019; Bechtold et al., 2018). Even fewer studies have assessed the combined use of optical and SAR imagery in peatland wetness monitoring, and most of them have used only NDVI from optical imagery (Holtgrave et al., 2018; Dabrowska-Zielinska et al., 2018; Millard et al., 2018). Only in one study, optical Sentinel-2 data was used more versatilely and was combined with Landsat thermal and Sentinel-1 SAR data (Klinke et al., 2018).

Here, we monitored peatland WTD data from 50 restored and undrained peatland study sites using optical (Landsat 5–8 and Sentinel-2) and C-band SAR (Sentinel-1) satellite imagery. Using multi-annual *in-situ* WTD data as a reference, we asked how well WTD can be monitored with remote sensing data, whether multi-sensor approach boosts explanatory capacity, and if there are differences in regression performance between sensor types, peatland habitat types, and between undrained and restored sites.

2. Methods

2.1. Study sites and water table depth data

We included 50 study sites in the analysis, located between 60° and 66° N in Finland (Fig. 1, Table S1). Each site is represented by one WTD monitoring point located within a larger peatland complex. Six of the sites are included in the Natural Resources Institute Finland peatland restoration monitoring network (Tolvanen et al., 2020) while the rest 44 sites are included in the Parks & Wildlife Finland (Metsähallitus) permanent monitoring network of restored peatlands. We divided the sites into three different peatland habitat types (spruce mires, pine mires, and open mires) and two management options (restored and undrained) (Table 1). All sites had peat depths > 30 cm.

Spruce mires are minerotrophic peatlands with abundant tree cover, main tree species being Norway spruce (*Picea abies*) and Downy birch (*Betula pubescens*). Field layer is mostly covered by forbs and shrubs while feather mosses and *Sphagnum* cover the ground layer. The mean (±standard deviation) WTD in the monitoring data was 15 ± 10 cm and 24 ± 13 cm for the undrained and restored sites, respectively (Table S1). Pine mires have sparser tree cover and are nutrient-poorer than spruce mires. Main tree species is Scots pine (*Pinus sylvestris*). Field layer is dominated by shrubs and ground layer by *Sphagnum* mosses. WTD was 13 ± 5 cm and 19 ± 6 cm for the undrained and restored sites, respectively. Open mires have few to no trees and are highly heterogeneous in their nutrient status and in the field and ground layer vegetation. While some sites are dominated by shrubs and *Sphagnum*, some are sedge and wet brown moss dominated. WTD for the undrained and restored sites was 13 ± 4 cm and 16 ± 4 cm, respectively.

The restored sites had been drained for forestry between 1950 s and 1970 s and restored by filling the ditches and cutting the tree stand to mimic the pre-drainage state between 2007 and 2013. The area of restoration measures around the monitoring plots ranged between 1 and 24 ha (mean 6 ha). The undrained peatlands were not heavily affected by human management but might have dried partially due to drainage of adjacent peatland areas (Kolari et al., 2021; Sallinen et al., 2019).

We obtained WTD monitoring data collected with automatic loggers for each site. The measurements were conducted with Solinst Leveloggers and InTech TruTrack loggers, and the raw data were converted into WTD by taking the nearby air pressure (Solinst Leveloggers) or measurement depth (InTech TruTrack) into account. The data was collected either every four hours or half-hourly, and we calculated for each site the mean WTD per day for the snow-free period between May and October for further analyses.

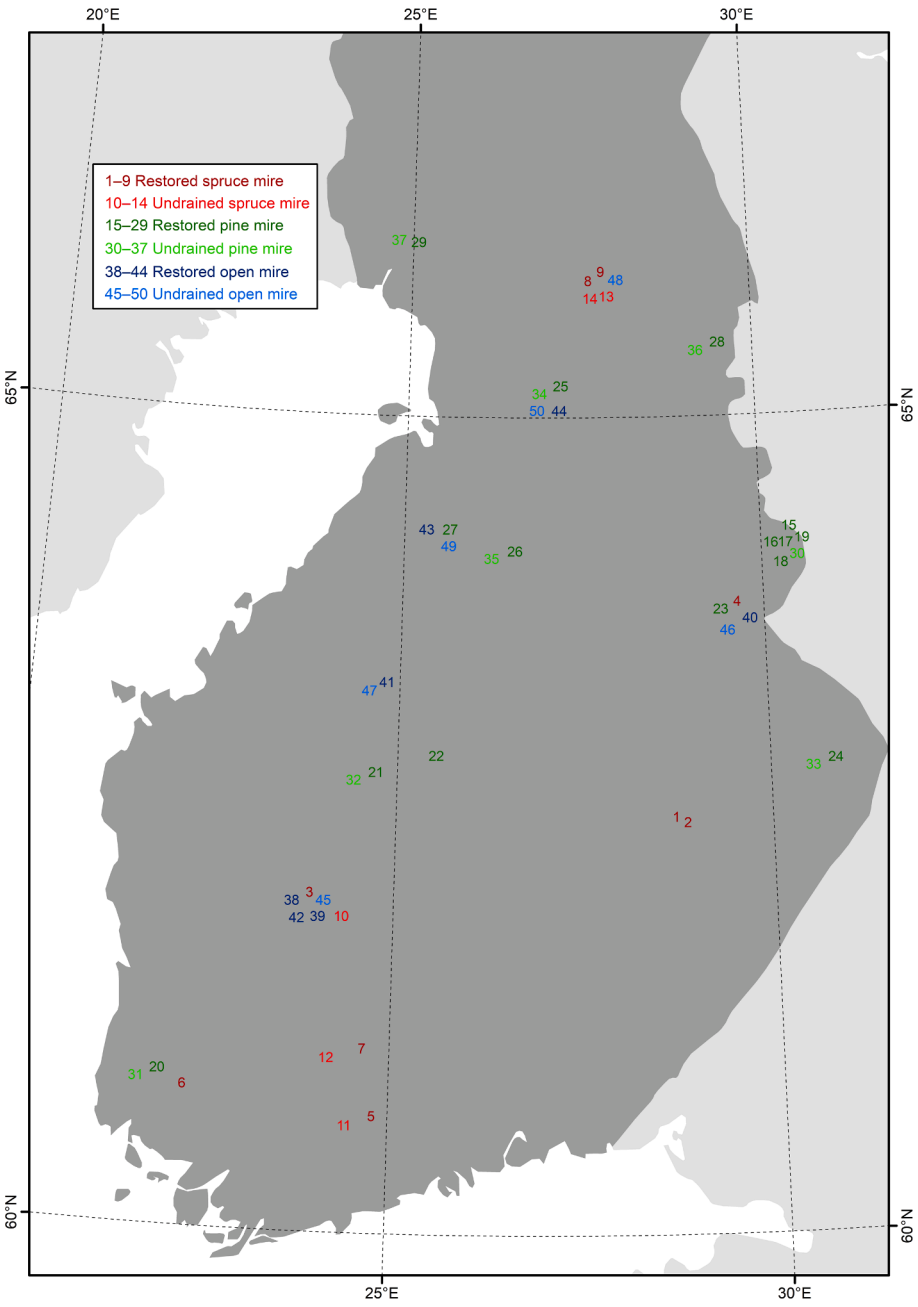

Fig. 1. The location of the study sites within southern Finland. The numbers refer to specific sites which are detailed in Table S1.

Table 1
Number of study sites for each habitat type and management option.

		Management options		In total
		Restored	Undrained	
Habitat types	Spruce mire	9	5	14
	Pine mire	15	8	23
	Open mire	7	6	13
In total		31	19	50

2.2. Satellite imagery and its preprocessing

We applied a 25 m radius buffer around each WTD monitoring site and calculated temporal trends for selected optical and C-band SAR metrics (Table 2) for each year between May and October in Google Earth Engine (Gorelick et al., 2017). We calculated the mean value for each metric within the buffered area. The 25 m buffer was selected so that it included multiple pixels to remove noise from the data but so that it was a relatively homogeneous area within the focal peatland and excluded other land cover or habitat types or management options.

In the optical image analysis, we used Landsat 5–8 and Sentinel-2 surface reflectance data with the following bands: blue, green, red, NIR, SWIR1 (~1600 nm) and SWIR2 (~2200 nm). Landsat data was available over the whole monitoring period, while Sentinel-2 data was available since May 2017. We harmonized all datasets to match with Landsat 8 OLI bands (Zhang et al., 2018; Roy et al., 2016). We selected only images with maximum cloud cover 20% and masked remaining clouds. Gaps in the Landsat 7 data caused by the scan line failure were filled with a fixed 300 m square kernel. We calculated 21 indices for each image, each of which has been judged relevant for wetness or wet area detection (Table 2). Of the chosen indices, parameterization is required for OPTRAM and exponentially fitted OPTRAM ($OPTRAM_{exp}$).

Table 2
Explanatory variables calculated from optical and C-band SAR data. Justification and reference to each variable is given in Table S2.

Type	Variable (and used bands)	Abbreviation
Optical	Angle based drought index 1 (NIR, SWIR1)	ABDI1
	Angle based drought index 1 (NIR, SWIR2)	ABDI2
	Blue reflectance	Blue
	Difference vegetation index (red, NIR)	DVI
	Green difference vegetation index (green, NIR)	GDVI
	Green reflectance	Green
	Modified normalized difference water index (green, SWIR1)	MNDWI
	Modified normalized difference water index 2 (green, SWIR2)	MNDWI2
	Normalized difference moisture index (NIR, SWIR1)	NDMI
	Normalized difference moisture index 2 (NIR, SWIR2)	NDMI2
	Normalized difference vegetation index (green, NIR)	NDVI
	Normalized difference water index (red, NIR)	NDWI
	Near-infrared reflectance	NIR
	Normalized multi-band drought index (NIR, SWIR1. SWIR2)	NMDI
	Optical trapezoid model (red, NIR, SWIR2)	OPTRAM
	Exponentially fitted optical trapezoid model (red, NIR, SWIR2)	$OPTRAM_{exp}$
	Red reflectance	Red
	Shortwave infrared transformed reflectance (SWIR2)	STR
	Shortwave infrared band 1 reflectance	SWIR1
	Shortwave infrared band 2 reflectance	SWIR2
	Visible and shortwave infrared drought index (blue, red, SWIR1)	VSDI
SAR	Original VH backscatter	VH
	Incidence angle corrected VH backscatter	VH_{angle}
	Sine corrected VH backscatter	VH_{sine}
	Original VV backscatter	VV
	Incidence angle corrected VV backscatter	VV_{angle}
	Sine corrected VV backscatter	VV_{sine}
	Normalized polarization ((VH-VV) / (VH + VV)) of original, angle corrected, and sine corrected VH and VV data, respectively	Pol Pol_{angle} Pol_{sine}
	Incidence angle	Angle

Following earlier studies (Burdun et al., 2020; Ambrosone et al., 2020; Babaeian et al., 2018; Sadeghi et al., 2015), we visually interpreted STR-NDVI space that included all pixels for each monitoring site buffer area and time point and assigned linear (OPTRAM) or exponential ($OPTRAM_{exp}$) threshold lines for the dry and wet edges.

In SAR image analysis, we utilized ground range detected Sentinel-1 data available since October 2014. To secure data consistency, we included data only from ascending orbit. We followed the preprocessing steps by (Mullissa et al., 2021); in other words, we applied additional border noise correction, reduced speckle with multi-temporal (Quegan and Jiong Jiong, 2001) Lee Sigma filter (Jong-Sen Lee et al., 2009) with kernel size and number of images set to 5 and conducted radiometric terrain normalization utilizing National Land Survey of Finland 10 m spatial resolution digital terrain model and converted the data to decibels. We calculated 10 SAR metrics for each image (Table 2). The angle and sine correction were calculated using the equations by (Lees et al., 2021) who developed the equation for open peatland ecosystems in Great Britain. We modified the sine correction equation to match to a typical Finnish growing season so that the correction was close to 0 at doy 140 (approximate start of growing season) and 277 (approximate end of growing season) and close to maximum value of 1 at doy 208 (approximate peak of growing season) (equation (1)).

$$\sigma^{\circ}_{sine} = \sigma^{\circ}_{angle} - \sin(0.023 \times (doy - 140)) \quad (1)$$

In which σ°_{sine} and σ°_{angle} are sine and angle corrected backscatter coefficients (in decibels), respectively, and *doy* is the day of the year of image acquisition. We tested the sine correction on our data, and it increased the correlation between WTD and VV backscatter on average by 14 %-points.

In some cases, erroneous observations may exist particularly in the optical data that is sensitive to weather even though clouds are masked from the data. To identify and replace outliers, we used Friedman's super smoother (Friedman, 1984) separately for each metric and site.

2.3. Statistical analyses

To assess how well the temporal trends in WTD can be predicted with remote sensing data, we ran separate random forest regressions (Breiman, 2001) for each study site (N = 50) with the dependent variable being the measured daily WTD and independent variables consisting of remote sensing metrics (Table 2, Fig. 2). Additionally, we implemented combined models for the habitat type and management option combinations (N = 6) in which data from several study sites were lumped together.

We used random forest, an ensemble of bootstrapped classification and regression trees, which has functioned well in remote sensing analyses with multiple collinear explanatory variables and with temporal data and reported to be insensitive to overfitting (Douna et al., 2021; Belgiu and Drăguţ, 2016). We set the number of trees to 500 and number of variables tested at each tree node to the square root of available variables (Belgiu and Drăguţ, 2016). To boost regression performance, to further avoid overfitting, and to remove irrelevant variables, we conducted genetic algorithm variable selection (Kuhn and Johnson, 2013; Scrucca, 2013) with five-fold cross-validation and three iteration rounds before implementing the final regression models.

In random forest, when each tree is built, roughly two thirds of data is randomly sampled for training while the remaining one third (out-of-bag) is left for validation and calculating variable importance. We assessed model performance with the out-of-bag evaluation, which has been reported to be a conservative estimate of model fit when compared to an independent test set (Clark et al., 2010). We calculated the % of explained variance (i.e., random forest pseudo R^2 = 1 - mean square error / variance of dependent variable) and normalized root mean square error (nRMSE; RMSE divided by the range of dependent variable values) for each site. To analyze differences between peatland habitat types and management options, we grouped the sites into three peatland habitat types (spruce mires, pine mires, open mires) and two management options (restored, undrained) and calculated mean R^2 and nRMSE and other statistics for the groups.

We calculated variable importance using the random forest mean decrease accuracy score from the regressions for which variables were chosen with genetic algorithms. To increase the cross-comparability of different variables between study sites, we normalized the variable importance scores with a min–max method to 0–1 scale for each site and then summed the normalized values for different peatland habitat types and management options.

In our main analysis, we combined the data to include WTD, optical and C-band SAR data for the same dates. We included those days in the analysis that had optical data. For each day, we included data only from one optical sensor. We then searched for the closest SAR date acquisition date for each day with optical data with a maximum seven-day difference. We decided to filter the data based on optical data availability due to higher temporal resolution of SAR data. The number of WTD observations per each site ranged from 20 to 71 (mean 39, Table S1). For this dataset, we conducted regressions with three explanatory variable options: (1) variables from both sensor types, (2) optical variables only, and (3) C-band SAR variables only. To test the robustness of the analysis, we also run regressions for the whole optical (33–127 observations per site; mean 81) and C-band SAR (60–266 observations per site; mean 145) datasets (Table S1). For the optical analysis, this prolonged the monitoring period for the whole time with WTD data. For the SAR analysis, this increased the amount of data points per year and allowed to use the WTD data for the exact days with SAR data acquisition.

The analyses were conducted in R with packages randomForest, caret and forecast.

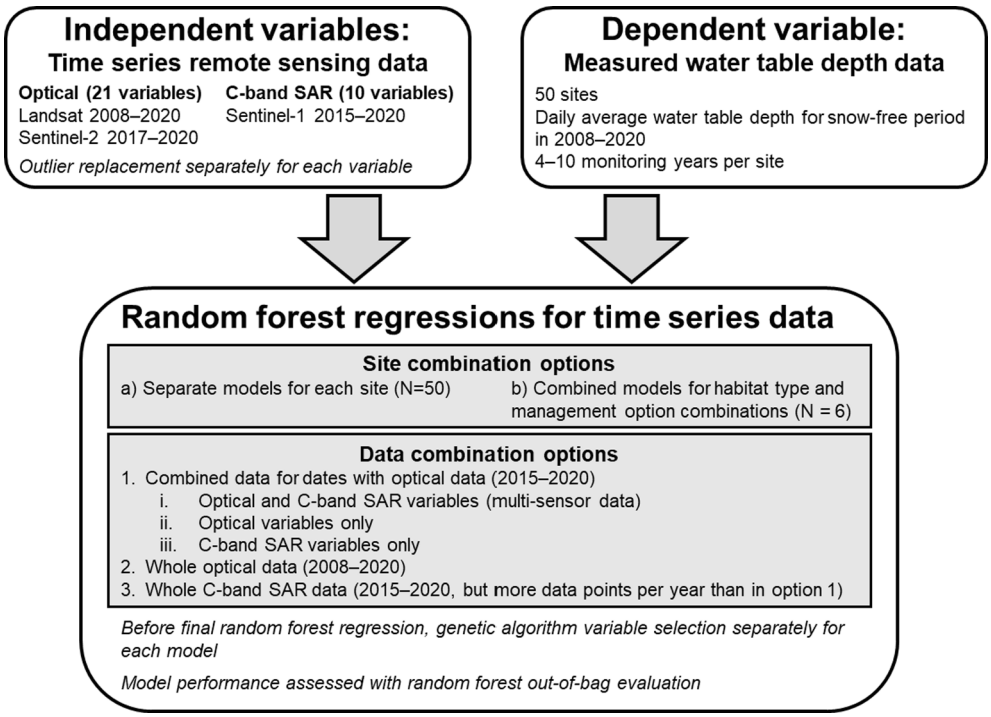

Fig. 2. Methodological flowchart.

3. Results

The mean explained variance and nRMSE were 42.7% and 19.8%, respectively, when the regressions were applied separately for each site and explanatory variables included both optical and C-band SAR metrics. The results were almost equal for the models with optical variables only (R^2 42.1% and nRMSE 19.9%) but notably lower for the models with SAR variables only (R^2 20.8% and nRMSE 23.6%). When the models combined data from several sites, the mean performance of C-band SAR data models (R^2 33.7% and nRMSE 15.3%) was closer to that of optical models (R^2 36.6% and nRMSE 15.0%), while multi-sensor models had considerably higher performance (R^2 40.6% and nRMSE 14.5%) (Table 3, Fig. 3).

Despite these general patterns, the models with C-band SAR data only had higher performance than other models at some study sites and higher performance than the optical models for the models combining data from several restored open mires or restored spruce mires. Furthermore, there was a significant variation in regression performance between peatland habitat types and management options, and even higher variation within some of the types (Fig. 4). In general, the performance was higher for open and pine mires than for spruce mires and higher for undrained than for restored peatlands (Table 3, Fig. 4). In the whole optical and C-band SAR datasets with separate models for each site, the general trends remained similar, with optical data (mean R^2 38.1% and nRMSE 18.8%) having higher performance than C-band SAR data (mean R^2 24.1% and nRMSE 19.8%).

When summed over all sites, the most important variable in the models run separately for each site and including multi-sensor data were $OPTRAM_{exp}$, SWIR1, VV_{sine}, OPTRAM and DVI (Fig. 5) There was considerable variation between sites as well as between peatland habitat types and management options concerning which variables were deemed the most important. For instance, even though SWIR1 and OPTRAM variables had the highest overall importance, they were rejected by the genetic algorithm at some sites. For instance, $OPTRAM_{exp}$ was rejected at all restored open mire sites (Fig. 5). Apart from sine corrected backscatter, almost all optical variables were deemed more important than C-band SAR variables, and many of the optical variables had almost equally high overall importance values. For the models combining data from several sites, the most important variable was NMDI followed by SWIR1, OPTRAM, $OPTRAM_{exp}$ and VV_{sine} (Fig. S1). On average, 12 and 17 variables were deemed important by genetic algorithms in multi-sensor models trained separately for each site and combining data from several sites, respectively.

Table 3
Percentage of variance explained (% Var) and normalized root mean square error (nRMSE) for models combining data from several sites. Models were run separately with multi-sensor data (combination of optical and C-band SAR), optical data, and C-band SAR data. Average values for models with multi-sensor data, optical data and C-band SAR data are indicated in the bottom row.

Habitat type	Management option	Multi-sensor		Optical		SAR	
		% Var	nRMSE (%)	% Var	nRMSE (%)	% Var	nRMSE (%)
Open mire	Undrained	49.07	11.91	45.86	12.28	38.22	13.12
	Restored	39.01	15.14	32.95	15.87	37.62	15.31
Pine mire	Undrained	47.45	12.21	47.04	12.26	39.76	13.07
	Restored	38.42	14.02	32.48	14.68	30.69	14.88
Spruce mire	Undrained	34.74	15.07	30.70	15.53	24.89	16.17
	Restored	35.07	18.62	30.63	19.25	30.87	19.22
Average		40.63	14.50	36.61	14.98	33.68	15.29

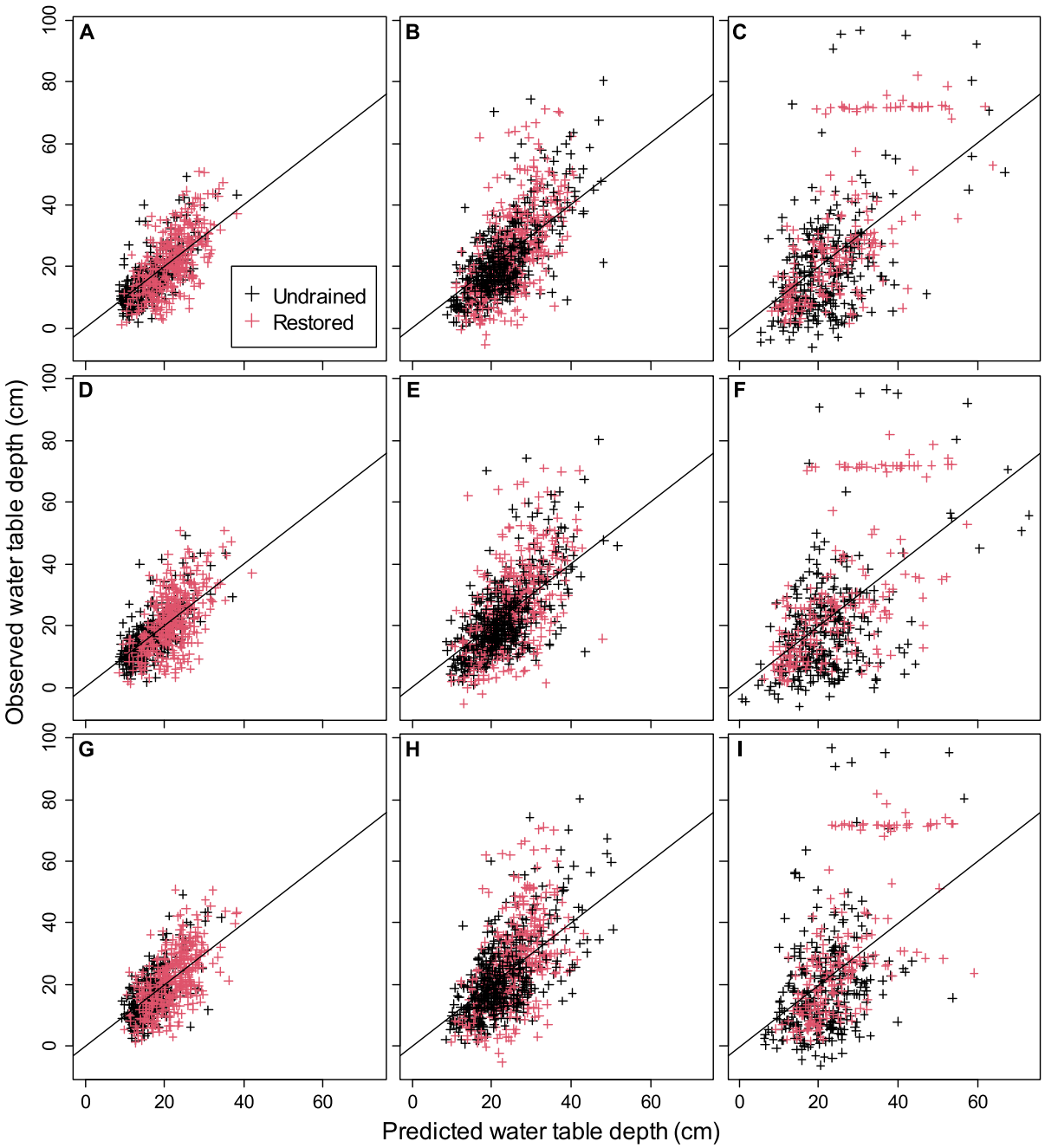

Fig. 3. Observed (y-axis) and predicted (x-axis) water table depths for open mire (A, D, G), pine mire (B, E, H), and spruce mire (C, F, I) models with multi-sensor data (A-C), optical data (D-F), and C-band SAR data (G-I). Black line is 1:1 line. Predicted values are based on the models which included data from several sites and were trained separately for the different habitat types and management options. Model performance results are presented in Table 3. Note that observations and predictions for undrained (black symbols) and drained peatland sites (red symbols) are drawn in the same figures.

4. Discussion and conclusions

Our results show that there is no one-size-fits-all approach for detecting WTD and soil moisture in peatlands. There are large differences between and within peatland habitat types and management options in how well WTD can be tracked. Moreover, multi-sensor approach boosts explanatory capacity moderately little, and optical data works usually better than does C-band SAR data.

The % of explained variance averaged over all sites was relatively similar when compared to earlier studies that have reported the squared correlation or coefficient of determination between spaceborne remote sensing variables and WTD or soil moisture to be 0.02 to 0.93 and often < 0.50 (Burdun et al., 2020; Burdun et al., 2020; Holtgrave et al., 2018; Lees et al., 2021; Asmuß et al., 2019; Torbick et al., 2012; Bechtold et al., 2018; Kim et al., 2017; Klinke et al., 2018). However, a higher overall performance could have been expected due to the applied machine learning-based multi-sensor approach.

There was a large range of values in % of explained variance. This finding is supported by earlier studies that show a similar variation in remote sensing based WTD or soil moisture estimation at different sites (Burdun et al., 2020; Holtgrave et al., 2018; Lees et al., 2021; Asmuß et al., 2019; Millard and Richardson, 2018); however, the previous studies utilized data only from a limited number of sites. The most evident explanation for the high variation is the differences between sites. Our results show that the regression performance is on average lower at densely treed and relatively dry sites (spruce mires) than on

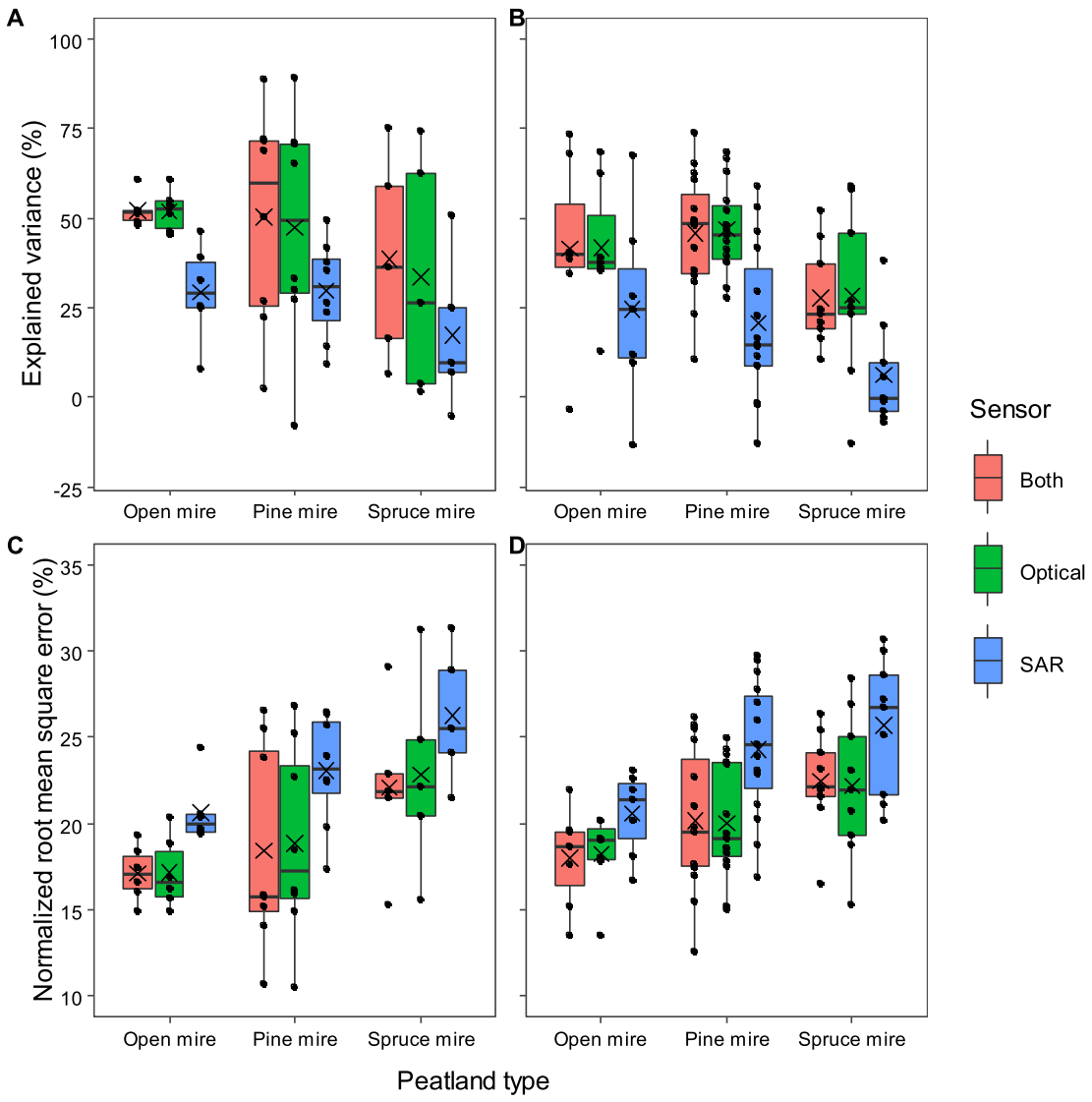

Fig. 4. The % of explained variance (A, B) and normalized root mean square error (C, D) boxplots for undrained (A, C) and restored (B, D) peatland sites. Separate boxplots are shown for models having variables from both sensor types, optical data, and C-band SAR data, as well as for the three peatland habitat types. Median value is shown with the center line, and first and third quartiles with lower and upper hinges, respectively. Whiskers extend to the smallest and largest value no further than 1.5 times the interquartile range from the hinge. Each dot in the boxplot is the statistic value for one peatland site while mean value for a boxplot is shown with "x".

wetter and treeless or sparsely treed sites. This result is in line with earlier studies that show that WTD and soil moisture estimations function better at open areas lacking trees that hamper the optical (Burdun et al., 2020) or SAR signals (Millard and Richardson, 2018). Furthermore, at the drier sites, there might be weaker relationship between WTD and surface moisture (Kellner and Halldin, 2002) which hampers the ability to track WTD with remote sensing. Nonetheless, our results also show the high variation within densely treed, sparsely treed, and open peatland habitat types.

The results showed that regression performance is on average higher in undrained peatlands than in study sites that have experienced recent restoration. In our main analyses, the restoration work was implemented 1–10 years before the start of the observation period. The disturbance phase of the restoration process usually takes several years (Tolvanen et al., 2020; Haapalehto et al., 2017) affecting the surface vegetation and hydrology, which may hamper remote sensing studies. At the same time, for open and semi-open peatland habitat types, most or part of the tree stand is usually removed as a restoration action, potentially facilitating remote sensing monitoring. Overall, the poorer explanatory capacity in restored sites is unfortunate because there is a high need to develop objective monitoring measures for peatland restoration success (Andersen et al., 2017; Chimner et al., 2017).

Optical remote sensing data had higher variable importance scores, and models with optical data higher regression performance than C-band SAR data. Nevertheless, in the models including data from several sites, the difference between optical and C-band SAR data was smaller than in the average performance of separate models for each site. The inferiority of C-band SAR data compared to optical data is rather surprising because C-band SAR has some penetration capability through the vegetation and microwaves are sensitive to the dielectric constant (and thus to the water content) of the observed targets (Li et al., 2021). However, the result could have been different if SAR data would have been acquired with a greater vegetation and soil permittivity, e.g. from L-band (Li et al., 2021). Therefore, our results cannot be generalized to all SAR data.

When looking at earlier peatland research, a direct comparison in optical versus SAR performance is complicated due to the lack of comparative studies. The low overall performance of quad-polarization

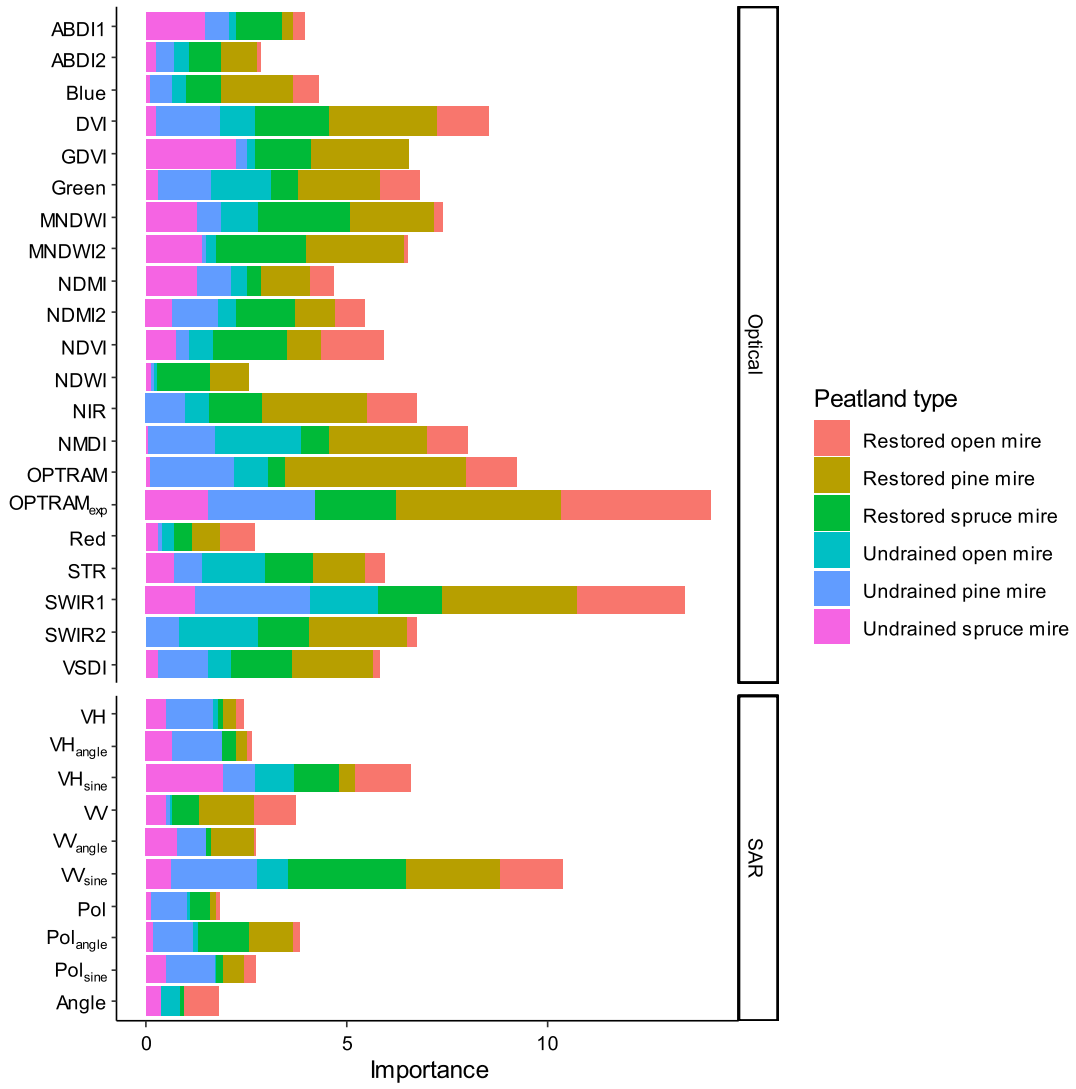

Fig. 5. Variable importance for the models with explanatory variables calculated from multi-sensor data (combination of optical and C-band SAR data). The boxes represent summed variable importance over all sites. Variable names are explained in Table 2.

C-band SAR has been reported in some of the earlier studies (Millard et al., 2018) while other studies show high performance of C-band SAR with VH or VV polarization (Lees et al., 2021; Manninen et al., 2022) and others intermediate performance with a high variation between sites with HH, HV, VH, and VV polarizations (Asmuß et al., 2019; Millard and Richardson, 2018). In studies utilizing optical sensors, similar variation in regression performance variation can be found. Some report high explanatory capacities, in particular with airborne hyperspectral or field spectroscopy narrowband indices or more sophisticated analysis methods, such as wavelet decomposition (Kalacska et al., 2018; Meingast et al., 2014; Banskota et al., 2017), while others, in particular multispectral satellite-based studies report intermediate performance (Burdun et al., 2020; Burdun et al., 2020), and some do not even find statistically significant correlation between field-spectroscopy-based indices and wetness (Lees et al., 2020).

Our results highlight that different remote sensing indices, sensors, and their combinations function well at different sites. Of the optical bands and indices, SWIR and NIR bands and indices calculated utilizing these bands had high variable importance. Earlier studies have emphasized in particular the importance of SWIR region (Kalacska et al., 2018; Meingast et al., 2014; Harris and Bryant, 2009). On the one hand, the relatively high importance of $OPTRAM_{exp}$ and OPTRAM was not surprising in light of earlier studies (Burdun et al., 2020; Burdun et al., 2020; Ambrosone et al., 2020; Sadeghi et al., 2017); on the other hand, the high importance of other optical metrics shows that OPTRAM is not a silver bullet. Of the C-band SAR metrics, sine corrected backscatter had the highest importance and VV variables were more important than VH variables. These results are backed by earlier research, which have shown that sine correction may increase correlation between backscatter and WTD almost 50% (Lees et al., 2021) and the superiority of VV over VH in soil moisture estimation (Asmuß et al., 2019) even though in peatland detection VH has outperformed VV (Räsänen et al., 2021; Karlson et al., 2019). The relatively low importance of normalized polarization has also been reported earlier (Hird et al., 2017).

There are multiple possible research avenues for future studies. First, it has been shown that a best pixel approach (i.e., finding the most representative pixel or area within the focal peatland complex) enhances the explanatory capacity when using OPTRAM (Burdun et al., 2020). Corresponding results have also been reported in SAR studies suggesting that treeless patches within peatlands should be chosen for remote sensing-based soil moisture analyses (Millard and Richardson, 2018). When utilizing multi-sensor and multi-index data, the search for the most representative area can be tedious as the optimal area potentially differs between metrics and sensors; nevertheless, future research could develop methods for automated detection of suitable remote sensing sites or areas.

Second, ancillary environmental data for example on weather, topography, tree and other vegetation structure, and site characteristics helps to enhance explanatory capacity (Torbick et al., 2012; Millard et al., 2018), and some have reported that surface temperature data has functioned well in peatland soil moisture detection (Klinke et al., 2018; Wigmore et al., 2019; Luscombe et al., 2015). Also accounting for temporal autocorrelation could have given a boost. Some of these data can be collected from remote sensing sources, e.g., topography and vegetation structure information can be quantified with lidar data and surface temperature with satellite, airborne or drone-borne observations. It would be beneficial to test which additional data sources are most beneficial. Nonetheless, we decided to test how well WTD can be tracked with multitemporal spaceborne remote sensing data only and phenological changes in vegetation were accounted for in some of the predictors (e.g., OPTRAM, sine corrected backscatter) and by including vegetation indices as predictors.

Third, even though we used analysis-ready imagery, especially C-band SAR data could have been processed further for instance by using a more sophisticated model than sine equation to vegetation corrections (Santi et al., 2016; Paloscia et al., 2013; Dabrowska-Zielinska et al., 2018) or by using nonlocal filtering of pixel values (Manninen et al., 2022). Moreover, SAR interferometry could have brought additional information about seasonal surface height and WTD variation (Kim et al., 2017; Tampuu et al., 2020; Mohammadimanesh et al., 2018) and other SAR bands than C-band could have been included in the comparison. Finally, random forest approach could be compared to other machine or deep learning methods and regression approaches to assess the differences between models in terms of explanatory capacity and interpretability.

CRediT authorship contribution statement

Aleksi Räsänen: Conceptualization, Methodology, Validation, Formal analysis, Writing – original draft, Visualization. **Anne Tolvanen:** Resources, Writing – review & editing, Supervision. **Santtu Kareksela:** Conceptualization, Writing – review & editing, Project administration, Funding acquisition.

Declaration of Competing Interest

The authors declare that they have no known competing financial interests or personal relationships that could have appeared to influence the work reported in this paper.

Acknowledgements

The research was funded by the Ministry of the Environment and Natural Resources Institute Finland and supported by Parks & Wildlife Finland (Metsähallitus) through collecting data. We thank Lassi Päkkilä and Oili Tarvainen for processing the WTD data.

Appendix A. Supplementary data

Supplementary data to this article can be found online at https://doi.org/10.1016/j.jag.2022.102866.

References

Andersen, R., Farrell, C., Graf, M., Muller, F., Calvar, E., Frankard, P., Caporn, S., Anderson, P., 2017. An overview of the progress and challenges of peatland restoration in Western Europe. Restor. Ecol. 25 (2), 271–282.
Chimner, R.A., Cooper, D.J., Wurster, F.C., Rochefort, L., 2017. An overview of peatland restoration in North America: where are we after 25 years? Restor. Ecol. 25 (2), 283–292.
Chasmer, L., Mahoney, C., Millard, K., Nelson, K., Peters, D., Merchant, M., Hopkinson, C., Brisco, B., Niemann, O., Montgomery, J., Devito, K., Cobbaert, D., 2020a. Remote Sensing of Boreal Wetlands 2: Methods for Evaluating Boreal Wetland Ecosystem State and Drivers of Change. Remote Sensing 12 (8), 1321.
Chasmer, L., Cobbaert, D., Mahoney, C., Millard, K., Peters, D., Devito, K., Brisco, B., Hopkinson, C., Merchant, M., Montgomery, J., Nelson, K., Niemann, O., 2020b. Remote Sensing of Boreal Wetlands 1: Data Use for Policy and Management. Remote Sensing 12 (8), 1320.
Kellner, E., Halldin, S., 2002. Water budget and surface-layer water storage in a Sphagnum bog in central Sweden. Hydrol. Process. 16 (1), 87–103.
Strack, M., Price, J.S., 2009. Moisture controls on carbon dioxide dynamics of peat-Sphagnum monoliths. Ecohydrology: Ecosystems, Land and Water Process Interactions. Ecohydrogeomorphology 2 (1), 34–41.
Lafleur, P.M., Moore, T.R., Roulet, N.T., Frolking, S., 2005. Ecosystem respiration in a cool temperate bog depends on peat temperature but not water table. Ecosystems 8 (6), 619–629.
Babaeian, E., Sadeghi, M., Jones, S.B., Montzka, C., Vereecken, H., Tuller, M., 2019. Ground, Proximal, and Satellite Remote Sensing of Soil Moisture. Rev. Geophys. 57 (2), 530–616.
Li, Z.-L., Leng, P., Zhou, C., Chen, K.-S., Zhou, F.-C., Shang, G.-F., 2021. Soil moisture retrieval from remote sensing measurements: Current knowledge and directions for the future. Earth-Sci. Rev. 218, 103673.
Peng, J., Albergel, C., Balenzano, A., Brocca, L., Cartus, O., Cosh, M.H., Crow, W.T., Dabrowska-Zielinska, K., Dadson, S., Davidson, M.W.J., de Rosnay, P., Dorigo, W., Gruber, A., Hagemann, S., Hirschi, M., Kerr, Y.H., Lovergine, F., Mahecha, M.D., Marzahn, P., Mattia, F., Musial, J.P., Preuschmann, S., Reichle, R.H., Satalino, G., Silgram, M., van Bodegom, P.M., Verhoest, N.E.C., Wagner, W., Walker, J.P., Wegmüller, U., Loew, A., 2021. A roadmap for high-resolution satellite soil moisture applications – confronting product characteristics with user requirements. Remote Sens. Environ. 252, 112162.
Santi, E., Paloscia, S., Pettinato, S., Fontanelli, G., 2016. Application of artificial neural networks for the soil moisture retrieval from active and passive microwave spaceborne sensors. Int. J. Appl. Earth Obs. Geoinf. 48, 61–73.
Burdun, I., Bechtold, M., Sagris, V., Lohila, A., Humphreys, E., Desai, A.R., Nilsson, M.B., De Lannoy, G., Mander, Ü., 2020. Satellite Determination of Peatland Water Table Temporal Dynamics by Localizing Representative Pixels of A SWIR-Based Moisture Index. Remote Sensing 12 (18), 2936.
Kalacska, M., Arroyo-Mora, J., Soffer, R., Roulet, N., Moore, T., Humphreys, E., Leblanc, G., Lucanus, O., Inamdar, D., 2018. Estimating Peatland Water Table Depth and Net Ecosystem Exchange: A Comparison between Satellite and Airborne Imagery. Remote Sensing 10 (5), 687.
Burdun, I., Bechtold, M., Sagris, V., Komisarenko, V., De Lannoy, G., Mander, Ü., 2020. A Comparison of Three Trapezoid Models Using Optical and Thermal Satellite Imagery for Water Table Depth Monitoring in Estonian Bogs. Remote Sensing 12.
El Hajj, M., Baghdadi, N., Zribi, M., Bazzi, H., 2017. Synergic use of Sentinel-1 and Sentinel-2 images for operational soil moisture mapping at high spatial resolution over agricultural areas. Remote Sensing 9 (12), 1292.
Gao, Q.i., Zribi, M., Escorihuela, M., Baghdadi, N., 2017. Synergetic Use of Sentinel-1 and Sentinel-2 Data for Soil Moisture Mapping at 100 m Resolution. Sensors 17 (9), 1966.
Paloscia, S., Pettinato, S., Santi, E., Notarnicola, C., Pasolli, L., Reppucci, A., 2013. Soil moisture mapping using Sentinel-1 images: Algorithm and preliminary validation. Remote Sens. Environ. 134, 234–248.
Ambrosone, M., Matese, A., Di Gennaro, S.F., Gioli, B., Tudoroiu, M., Genesio, L., Miglietta, F., Baronti, S., Maienza, A., Ungaro, F., Toscano, P., 2020. Retrieving soil moisture in rainfed and irrigated fields using Sentinel-2 observations and a modified OPTRAM approach. Int. J. Appl. Earth Obs. Geoinf. 89, 102113.
Sadeghi, M., Babaeian, E., Tuller, M., Jones, S.B., 2017. The optical trapezoid model: A novel approach to remote sensing of soil moisture applied to Sentinel-2 and Landsat-8 observations. Remote Sens. Environ. 198, 52–68.
Bauer-Marschallinger, B., Paulik, C., Hochstöger, S., Mistelbauer, T., Modanesi, S., Ciabatta, L., Massari, C., Brocca, L., Wagner, W., 2018. Soil moisture from fusion of scatterometer and SAR: Closing the scale gap with temporal filtering. Remote Sens. 10 (7), 1030.
Wang, L., Qu, J.J., 2007. A normalized multi-band drought index for monitoring soil and vegetation moisture with satellite remote sensing. Geophys. Res. Lett. 34 (20).
Gao, B.-C., 1996. NDWI—A normalized difference water index for remote sensing of vegetation liquid water from space. Remote Sens. Environ. 58 (3), 257–266.
Zhang, N., Hong, Y., Qin, Q., Liu, L.u., 2013. VSDI: a visible and shortwave infrared drought index for monitoring soil and vegetation moisture based on optical remote sensing. Int. J. Remote Sens. 34 (13), 4585–4609.
Meingast, K.M., Falkowski, M.J., Kane, E.S., Potvin, L.R., Benscoter, B.W., Smith, A.M.S., Bourgeau-Chavez, L.L., Miller, M.E., 2014. Spectral detection of near-surface moisture content and water-table position in northern peatland ecosystems. Remote Sens. Environ. 152, 536–546.
Harris, A., Bryant, R.G., 2009. A multi-scale remote sensing approach for monitoring northern peatland hydrology: Present possibilities and future challenges. J. Environ. Manage. 90 (7), 2178–2188.
Šimanauskienė, R., Linkevičienė, R., Bartold, M., Dąbrowska-Zielińska, K., Slavinskienė, G., Veteikis, D., Taminskas, J., 2019. Peatland degradation: The relationship between raised bog hydrology and normalized difference vegetation index. Ecohydrology 12 (8).
D'Acunha, B., Lee, S.-C., Johnson, M.S., 2018. Ecohydrological responses to rewetting of a highly impacted raised bog ecosystem. Ecohydrology 11 (1), e1922.
McPartland, M.Y., Kane, E.S., Falkowski, M.J., Kolka, R., Turetsky, M.R., Palik, B., et al., 2019. The response of boreal peatland community composition and NDVI to hydrologic change, warming, and elevated carbon dioxide. Glob. Change Biol. 25 (1), 93–107.

Kolari, T.H.M., Sallinen, A., Wolff, F., Kumpula, T., Tolonen, K., Tahvanainen, T., 2021. Ongoing Fen-Bog Transition in a Boreal Aapa Mire Inferred from Repeated Field Sampling, Aerial Images, and Landsat Data. Ecosystems.

Ludwig, C., Walli, A., Schleicher, C., Weichselbaum, J., Riffler, M., 2019. A highly automated algorithm for wetland detection using multi-temporal optical satellite data. Remote Sens. Environ. 224, 333–351.

Holtgrave, A.-K., Förster, M., Greifeneder, F., Notarnicola, C., Kleinschmit, B., 2018. Estimation of Soil Moisture in Vegetation-Covered Floodplains with Sentinel-1 SAR Data Using Support Vector Regression. PFG – Journal of Photogrammetry, Remote Sensing and Geoinformation. Science 86 (2), 85–101.

Dabrowska-Zielinska, K., Musial, J., Malinska, A., Budzynska, M., Gurdak, R., Kiryla, W., Bartold, M., Grzybowski, P., 2018. Soil Moisture in the Biebrza Wetlands Retrieved from Sentinel-1 Imagery. Remote Sensing 10 (12), 1979.

Lees, K.J., Artz, R.R.E., Chandler, D., Aspinall, T., Boulton, C.A., Buxton, J., Cowie, N.R., Lenton, T.M., 2021. Using remote sensing to assess peatland resilience by estimating soil surface moisture and drought recovery. Sci. Total Environ. 761, 143312.

Manninen, T., Jaaskelainen, E., Lohila, A., Korkiakoski, M., Rasanen, A., Virtanen, T., Muhic, F., Marttila, H., Ala-Aho, P., Markovaara-Koivisto, M., Liwata-Kenttala, P., Sutinen, R., Hanninen, P., 2022. Very High Spatial Resolution Soil Moisture Observation of Heterogeneous Subarctic Catchment Using Nonlocal Averaging and Multitemporal SAR Data. IEEE Trans. Geosci. Remote Sens. 60, 1–17.

Asmuß, T., Bechtold, M., Tiemeyer, B., 2019. On the Potential of Sentinel-1 for High Resolution Monitoring of Water Table Dynamics in Grasslands on Organic Soils. Remote Sensing 11 (14), 1659.

Torbick, N., Persson, A., Olefeldt, D., Frolking, S., Salas, W., Hagen, S., Crill, P., Li, C., 2012. High Resolution Mapping of Peatland Hydroperiod at a High-Latitude Swedish Mire. Remote Sensing 4 (7), 1974–1994.

Bechtold, M., Schlaffer, S., Tiemeyer, B., De Lannoy, G., 2018. Inferring Water Table Depth Dynamics from ENVISAT-ASAR C-Band Backscatter over a Range of Peatlands from Deeply-Drained to Natural Conditions. Remote Sensing 10 (4), 536.

Millard, K., Thompson, D., Parisien, M.-A., Richardson, M., 2018. Soil Moisture Monitoring in a Temperate Peatland Using Multi-Sensor Remote Sensing and Linear Mixed Effects. Remote Sensing 10 (6), 903.

Millard, K., Richardson, M., 2018. Quantifying the relative contributions of vegetation and soil moisture conditions to polarimetric C-Band SAR response in a temperate peatland. Remote Sens. Environ. 206, 123–138.

Kim, J.-W., Lu, Z., Gutenberg, L., Zhu, Z., 2017. Characterizing hydrologic changes of the Great Dismal Swamp using SAR/InSAR. Remote Sens. Environ. 198, 187–202.

Kasischke, E.S., Bourgeau-Chavez, L.L., Rober, A.R., Wyatt, K.H., Waddington, J.M., Turetsky, M.R., 2009. Effects of soil moisture and water depth on ERS SAR backscatter measurements from an Alaskan wetland complex. Remote Sens. Environ. 113 (9), 1868–1873.

Sallinen, A., Tuominen, S., Kumpula, T., Tahvanainen, T., 2019. Undrained peatland areas disturbed by surrounding drainage: a large scale GIS analysis in Finland with a special focus on aapa mires. MIRES AND PEAT 24.

Klinke, R., Kuechly, H., Frick, A., Förster, M., Schmidt, T., Holtgrave, A.-K., Kleinschmit, B., Spengler, D., Neumann, C., 2018. Indicator-Based Soil Moisture Monitoring of Wetlands by Utilizing Sentinel and Landsat Remote Sensing Data. PFG – Journal of Photogrammetry, Remote Sensing and Geoinformation. Science 86 (2), 71–84.

Tolvanen, A., Tarvainen, O., Laine, A.M., 2020. Soil and water nutrients in stem-only and whole-tree harvest treatments in restored boreal peatlands. Restor. Ecol. 28 (6), 1357–1364.

Gorelick, N., Hancher, M., Dixon, M., Ilyushchenko, S., Thau, D., Moore, R., 2017. Google Earth Engine: Planetary-scale geospatial analysis for everyone. Remote Sens. Environ. 202, 18–27.

Zhang, H.K., Roy, D.P., Yan, L., Li, Z., Huang, H., Vermote, E., Skakun, S., Roger, J.-C., 2018. Characterization of Sentinel-2A and Landsat-8 top of atmosphere, surface, and nadir BRDF adjusted reflectance and NDVI differences. Remote Sens. Environ. 215, 482–494.

Roy, D.P., Kovalskyy, V., Zhang, H.K., Vermote, E.F., Yan, L., Kumar, S.S., Egorov, A., 2016. Characterization of Landsat-7 to Landsat-8 reflective wavelength and normalized difference vegetation index continuity. Remote Sens. Environ. 185, 57–70.

Babaeian, E., Sadeghi, M., Franz, T.E., Jones, S., Tuller, M., 2018. Mapping soil moisture with the OPtical TRApezoid Model (OPTRAM) based on long-term MODIS observations. Remote Sens. Environ. 211, 425–440.

Sadeghi, M., Jones, S.B., Philpot, W.D., 2015. A linear physically-based model for remote sensing of soil moisture using short wave infrared bands. Remote Sens. Environ. 164, 66–76.

Mullissa, A., Vollrath, A., Odongo-Braun, C., Slagter, B., Balling, J., Gou, Y., Gorelick, N., Reiche, J., 2021. Sentinel-1 SAR Backscatter Analysis Ready Data Preparation in Google Earth Engine. Remote Sensing 13 (10), 1954.

Quegan, S., Jiong Jiong, Y.u., 2001. Filtering of multichannel SAR images. IEEE Trans. Geosci. Remote Sens. 39 (11), 2373–2379.

Jong-Sen Lee, Jen-Hung Wen, Ainsworth, T.L., Kun-Shan Chen, Chen, A.J., 2009. Improved Sigma Filter for Speckle Filtering of SAR Imagery. IEEE Trans. Geosci. Remote Sens. 47 (1), 202–213.

Friedman, J.H., 1984. A variable span scatterplot smoother. Laboratory for Computational Statistics, Stanford University Technical Report No. 5.

Breiman, L., 2001. Random Forests. Mach Learning 45 (1), 5–32.

Douna, V., Barraza, V., Grings, F., Huete, A., Restrepo-Coupe, N., Beringer, J., 2021. Towards a remote sensing data based evapotranspiration estimation in Northern Australia using a simple random forest approach. J. Arid Environ. 191, 104513.

Belgiu, M., Drăguţ, L., 2016. Random forest in remote sensing: A review of applications and future directions. ISPRS J. Photogramm. Remote Sens. 114, 24–31.

Kuhn, M., Johnson, K., 2013. Applied Predictive Modeling. Springer New York, New York, NY.

Scrucca, L., 2013. GA: A Package for Genetic Algorithms in R. J. Stat. Softw. 53 (4), 1–37.

Clark, M.L., Aide, T.M., Grau, H.R., Riner, G., 2010. A scalable approach to mapping annual land cover at 250 m using MODIS time series data: A case study in the Dry Chaco ecoregion of South America. Remote Sens. Environ. 114 (11), 2816–2832.

Haapalehto, T., Juutinen, R., Kareksela, S., Kuitunen, M., Tahvanainen, T., Vuori, H., Kotiaho, J.S., 2017. Recovery of plant communities after ecological restoration of forestry-drained peatlands. Ecol. Evol. 7 (19), 7848–7858.

Banskota, A., Falkowski, M.J., Smith, A.M.S., Kane, E.S., Meingast, K.M., Bourgeau-Chavez, L.L., Miller, M.E., French, N.H., 2017. Continuous Wavelet Analysis for Spectroscopic Determination of Subsurface Moisture and Water-Table Height in Northern Peatland Ecosystems. IEEE Trans. Geosci. Remote Sens. 55 (3), 1526–1536.

Lees, K.J., Artz, R.R.E., Khomik, M., Clark, J.M., Ritson, J., Hancock, M.H., Cowie, N.R., Quaife, T., 2020. Using Spectral Indices to Estimate Water Content and GPP in *Sphagnum* Moss and Other Peatland Vegetation. IEEE Trans. Geosci. Remote Sens. 58 (7), 4547–4557.

Räsänen, A., Manninen, T., Korkiakoski, M., Lohila, A., Virtanen, T., 2021. Predicting catchment-scale methane fluxes with multi-source remote sensing. Landscape Ecol. 36 (4), 1177–1195.

Karlson, M., Gålfalk, M., Crill, P., Bousquet, P., Saunois, M., Bastviken, D., 2019. Delineating northern peatlands using Sentinel-1 time series and terrain indices from local and regional digital elevation models. Remote Sens. Environ. 231, 111252.

Hird, J., DeLancey, E., McDermid, G., Kariyeva, J., 2017. Google Earth Engine, Open-Access Satellite Data, and Machine Learning in Support of Large-Area Probabilistic Wetland Mapping. Remote Sensing 9 (12), 1315.

Wigmore, O., Mark, B., McKenzie, J., Baraer, M., Lautz, L., 2019. Sub-metre mapping of surface soil moisture in proglacial valleys of the tropical Andes using a multispectral unmanned aerial vehicle. Remote Sens. Environ. 222, 104–118.

Luscombe, D.J., Anderson, K., Gatis, N., Grand-Clement, E., Brazier, R.E., 2015. Using airborne thermal imaging data to measure near-surface hydrology in upland ecosystems. Hydrol. Process. 29 (6), 1656–1668.

Tampuu, T., Praks, J., Uiboupin, R., Kull, A., 2020. Long Term Interferometric Temporal Coherence and DInSAR Phase in Northern Peatlands. Remote Sensing 12 (10), 1566.

Mohammadimanesh, F., Salehi, B., Mahdianpari, M., Brisco, B., Motagh, M., 2018. Wetland Water Level Monitoring Using Interferometric Synthetic Aperture Radar (InSAR). A Review. null 44 (4), 247–262.